

# Tracer particle transport dynamics in the diffusive sandpile cellular automaton

J.A. Mier<sup>a1</sup>, R. Sanchez<sup>b</sup> and D. E. Newman<sup>c</sup>

<sup>a</sup>*Departamento de Física Aplicada, Universidad de Cantabria, 39005 Santander, Spain*

<sup>b</sup>*Departamento de Física, Universidad Carlos III de Madrid, 28911 Leganés, Madrid, Spain*

<sup>c</sup>*Department of Physics, University of Alaska, Fairbanks, AK 99775-5920, USA*

---

## Abstract

The confinement properties of the diffusive running sandpile are characterized by tracking the motion of a population of marked grains of sand. It is found that, as the relative strength of the avalanching to the diffusive transport channel is varied, a point is reached at which the particle global confinement time and the probability density functions of the jump-sizes and waiting-times of the tracked grains experience a sudden change, thus revealing a dynamical transition, that is consistent with previous studies (Newman DE et al., Phys Rev Lett 2002;88(20):204304). Across this transition, the sandpile moves from a regime characterized by self-similarity and memory, where avalanches of all possible sizes dominate transport across the system, to another regime where transport is taken over by near system-size, quasi-periodic avalanches. Values for the fractional transport exponents that quantify effective transport across the sandpile prior to the transition are also obtained.

*Keywords:* Diffusive Sandpile; tracer particles; Self-Organized Criticality; fractional transport.

---

## 1. Introduction

Many studies have relied on the concept of self-organized criticality [1] (SOC) as a possible explanation of the overall dynamics of a wide variety of

---

<sup>1</sup>Corresponding author. E-mail address: mierja@unican.es

physical and biological systems [2, 3, 4, 5, 6, 7, 8, 9]. All of them justify this hypothesis by the presence of the basic ingredients of SOC. Namely, an open driven system with a local instability threshold that drives local transport only when overcome, and a large disparity between the temporal scales associated to the drive and the instability relaxation. It is not difficult to find systems that fit into this type of description, at least approximately. The transport processes in them, often dominated by avalanches, are intrinsically bursty and exhibit a strong non-diffusive nature. In steady state, SOC systems exhibit properties such as spatial self-similarity, temporal persistence (memory effects) and long-term correlations, all typical of critical points at thermodynamical equilibrium. However, these properties appear here without any need for fine-tuning. Thus, its name: self-organized criticality.

The running sandpile automaton [10, 11] embodies many of the features often associated with SOC. It appeared simultaneously with the proposal of self-organized criticality and provides a simple paradigm to illustrate its dynamics. Many versions of the sandpile have appeared over the years, each tailored to specific applications. Of particular interest to us is the so-called diffusive running sandpile, first formulated in the context of magnetically confined fusion plasmas [12] with the purpose of understanding the dynamics of turbulent transport in situations where near-marginal turbulence coexisted with other types of (diffusive) transport [13]. The transport characteristics of the diffusive sandpile have been characterized in a number of ways over the years [14, 15, 16]. Its most remarkable features are that: 1) SOC features are maintained for finite, albeit small, strengths of the diffusive channel relative to the avalanche channel and 2) that, at larger values of their relative strength, a sudden transition takes place in which transport is no longer dominated by SOC-like avalanches, but by near-system wide global discharge events. It has been shown that this dynamical transition can be characterized in terms of a parameter that essentially measures the average roughness of the sandpile profile allowed by the transport taking place in the system [14].

In this paper we probe the nature of transport in the diffusive running sandpile by tracking the motion of a selected group of marked (or tracer) grains of sand. The trajectories of these grains are used to calculate the average particle confinement time, a well-known figure-of-merit for confinement quality in magnetically confined plasmas, as well as their jump-size and waiting-time probability density functions (pdfs). It will be shown that the transport dynamics can be well captured by these diagnostics both prior and

after the transition. Furthermore, the tracer data is also used to validate an effective transport model based on fractional transport equations [17] for the regime prior to the transition, that is the relevant one for confined plasmas, as well as to estimate the optimal values of the transport exponents that define this model.

The paper is thus organized as follows. First, the diffusive sandpile is reviewed in Sec. 2. Then, in Sec. 3, the rules that govern the motion of the tracers are presented and discussed. These rules are somewhat subtle since the diffusive channel does not distinguish individual grains. Next, the main results of the paper regarding tracer motion will be shown and discussed in Sec. 4. In 5, an effective transport model is validated and built for the diffusive sandpile steady state prior to the transition. The resulting transport equation contains fractional derivatives in space and time. The corresponding fractional exponents are also quantified numerically. Finally, some conclusions will be drawn in Sec. 6.

## 2. The diffusive sandpile model

The diffusive sandpile [12] is an extension of the standard one-dimensional running sandpile, but contains an additional diffusive transport channel whose intensity can be tuned relative to the avalanche-like one. The domain consists of  $L$  cells or sites, numbered from  $x = 1$  to  $x = L$ . The variable  $h(x, i)$  represents the height of sand at cell  $x$  at iteration  $i$  of the cellular automata. The evolution of the automata consists on randomly adding, at the beginning of each iteration, a grain of sand to every cell with probability  $P_0$ . Then, the avalanche dynamics are introduced by prescribing a critical slope value,  $-Z_c, Z_c > 0$ . Whenever the absolute value of the slope ( $|Z(x, i)| = |h(x + 1, i) - h(x, i)|$ ) exceeds this threshold ( $|Z(x, i)| > Z_c$ ),  $N_f$  grains of sand are moved from the unstable cell to the next one. All sandpile cells are checked for instability once per iteration.

Diffusive transport is introduced in the following way. A net diffusive flux is calculated as  $\Gamma_d(x, i) = -D_0 [Z(x - 1, i) - Z(x, i)] = \Gamma_d^+(x, i) - \Gamma_d^-(x, i)$  at each cell and iteration (see Fig. 1). This net flux is just the difference of the amount of sand that diffuses out of the previous cell at  $x - 1$  according to Fick's law,  $\Gamma_d^+(x, i) = -D_0 Z(x - 1, i)$ , and the amount of sand leaving the current cell diffusively to the next cell at  $x + 1$ ,  $\Gamma_d^-(x, i) = -D_0 Z(x, i)$ .  $D_0$  is a diffusion coefficient that is prescribed at the beginning of the run.

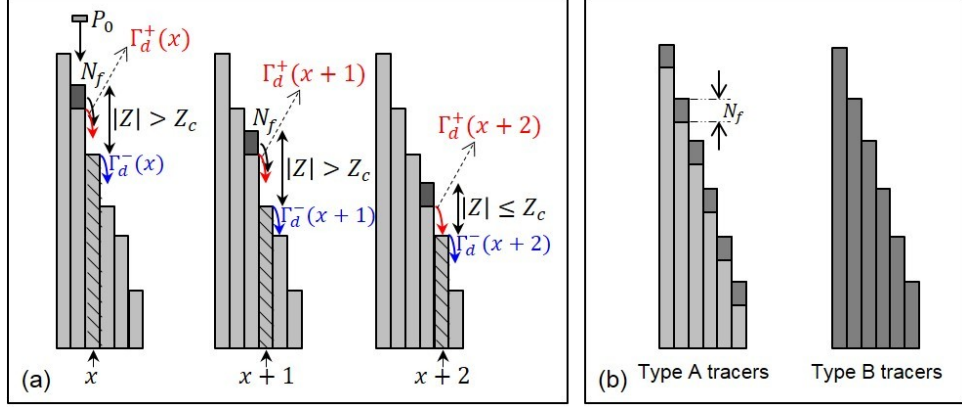


Figure 1: (a) Diagram explaining the one-dimensional diffusive sandpile automaton rules (the corresponding cell is filled with diagonal lines). Unlike the classical (non-diffusive) sandpile, a diffusive flux is incorporated to each cell now (see red and blue arrows). (b) Sketch showing the active tracer regions of the two formulations discussed in text. Type A tracers are confined in the top  $N_f$  positions in the cell. Type B tracers can be anywhere in the cell. The dark grey regions represent the possible locations of tracked particles for both cases.

Finally, the sandpile has a closed boundary at  $x = 1$  (no particles enter from the left), and an open boundary condition at  $x = L$  (particles reaching that cell are removed). The condition  $N_f > P_0 L - D_0 Z_a$  has to be fulfilled in order to avoid the sandpile become overdriven. Here,  $Z_a = Z_c - N_f/2$  is the averaged absolute value of the slope at the bottom edge cell [16, 18],  $x = L$ .

Under a constant drive (throughout this paper,  $P_0 \in [10^{-4} - 10^{-3}]$  has been used), the diffusive sandpile eventually reaches a steady state in which the incoming sand will balance (on average) the edge outflux. The diffusive sandpile domain is split into two regions connected at the intermediate cell  $x_t$ . The value of  $x_t$  is estimated as the outermost position at which the integrated source in the range  $[0, x_t]$ , i.e.,  $P_0 x_t$ , can still be entirely removed by diffusion while keeping the gradient below the minimum value accessed during avalanche activity in the SOC steady state [16], i.e.,  $|Z(x_t)| = Z_c - N_f$ . That is,

$$P_0 x_t \simeq D_0 (Z_c - N_f) \implies x_t \simeq \frac{D_0 (Z_c - N_f)}{P_0}. \quad (1)$$

$Z_c - N_f$  is used as the limiting value for the absolute value of the slope at  $x_t$  because it prevents any avalanche activity inwards: even if a toppling in the adjacent (to the right) cell happens, avalanche transport will be truncated at

$x_t$  since, in such a case,  $|Z(x_t, i + 1)| = |Z(x_t, i)| + N_f = Z_c - N_f + N_f = Z_c$ , which is just the limit to avoid avalanche propagation. In the region  $x < x_t$ , the absolute value of the slope is below  $Z_c$  and transport is entirely carried out through the diffusive channel. In the region  $x > x_t$ , transport is carried by both the diffusive and avalanche channels. The estimated values for  $Z_a$  and  $x_t$  agree well with simulations.

### 3. Advancing tracers in the diffusive sandpile

All marked sand grains are advanced simultaneously with the rest of sand grains in the sandpile. They are however treated differently in the sense that all tracers are transparent, not being accounted for when a cell is checked for instability or when updating the local sandpile height. Since the sandpile rules do not distinguish individual grains, the trajectory of a single tracer particle can in principle be defined in various ways, with the only restriction that they must be compatible with the sandpile governing rules. In this work, we examine only those grains that are contained within an active layer of depth  $N_f$  at the top of each cell, since we assume that those are the ones that are moved to the next cell as a result of an avalanche or diffusion [see dark grey regions in Fig. 1(b) for type A tracers].

If an avalanche happens and  $N_f$  grains must be moved to the next cell, they will necessarily be the ones closer to the surface of the cell. This situation resembles what takes place in a real sandpile, where only the grains closer to the surface are transported down the slope, whilst those more deeply buried stay trapped for very long times. However, other rules might be more appropriate for other systems. For instance, one could assume that any grain at a particular cell could move to the next cell as a result of an avalanche or of diffusive transport, independently of its relative depth within that cell [see dark grey regions in Fig. 1(b) for type B tracers]. We will not examine this case in this paper, though.

#### *Trajectories for tracked grains*

We proceed next to define exactly how tracers will be advanced. Each marked grain, labeled by the superindex  $m$ , is positioned at some initial time,  $t_0^m$ , at a prescribed cell,  $x_0^m$ . Within that cell, their depth from the top is set to  $d_0^m = uN_f$ , where  $u$  is a random number uniformly distributed in  $[0, 1]$ . As the sandpile evolves, the position,  $x^m$ , and depth,  $d^m$  of each marked grain are updated once the drive phase has been completed and the

stability for each cell checked. The specific rules used have been chosen to be consistent with both the macroscopic avalanching or diffusive channels that may transport them. They are as follows:

I) **Avalanche transport** [19, 18]:

- (1) If the current cell is stable ( $|Z| < Z_c$ ) and no grains of sand have been added during the driving phase, the tracer remains at the same cell,  
 $x^m(k) = x^m(k - 1)$ ,  
 and its depth remains unchanged,  
 $d^m(k) = d^m(k - 1)$ .
- (2) If the current cell is stable but one grain of sand has been dropped on it in the driving phase, the tracer remains in the same cell,  
 $x^m(k) = x^m(k - 1)$ ,  
 and its depth is increased by one,  
 $d^m(k) = d^m(k - 1) + 1$ .
- (3) If the current cell is stable, but the previous one is unstable and moves  $N_f$  grains over the current cell, the tracer remains in the same cell,  
 $x^m(k) = x^m(k - 1)$ ,  
 and its depth is increased by  $N_f$ ,  
 $d^m(k) = d^m(k - 1) + N_f$ .
- (4) If the current cell is stable, the previous one is unstable and, in the driving phase, one grain has fallen on the current cell, the tracer remains in the same cell,  
 $x^m(k) = x^m(k - 1)$ ,  
 and its depth is increased by  $N_f + 1$ ,  
 $d^m(k) = d^m(k - 1) + N_f + 1$ .
- (5) If the current cell is unstable (then  $N_f$  grains are moved to the following cell) and no grains have been dropped in the driving phase, then,
  - i. if the depth of the tracer is less or equal than  $N_f$ ,  $d^m(k - 1) \leq N_f$ , the tracer moves to the following cell,  
 $x^m(k) = x^m(k - 1) + 1$ ,  
 and its depth is initialized with a random value uniformly distributed in  $[0, N_f]$ ,  
 $d^m(k) = uN_f$ .

- ii. if the depth of the tracer is greater than  $N_f$ ,  $d^m(k-1) > N_f$ , the tracer remains in the same cell,
 
$$x^m(k) = x^m(k-1),$$
 and its depth is decreased by  $N_f$ ,
 
$$d^m(k) = d^m(k-1) - N_f.$$
- (6) If the current cell is unstable (then  $N_f$  grains are moved to the following cell) and one grain has been dropped in the driving phase, then,
  - i. if the depth of the tracer is less or equal than  $N_f - 1$ ,  $d^m(k-1) \leq N_f - 1$ , the tracer moves to the following cell,
 
$$x^m(k) = x^m(k-1) + 1,$$
 and its depth is initialized with a random value uniformly distributed in  $[0, N_f]$ ,
 
$$d^m(k) = uN_f.$$
  - ii. if the depth of the tracer is greater than  $N_f - 1$ ,  $d^m(k-1) > N_f - 1$ , the tracer remains in the same cell,
 
$$x^m(k) = x^m(k-1),$$
 and its depth is decreased by  $N_f - 1$ ,
 
$$d^m(k) = d^m(k-1) - (N_f - 1).$$

## II) Diffusive transport:

- (1) If the net diffusive flux in the current cell is negative and larger, in absolute value, than the tracer depth,  $D_0 d^2 h / dx^2 < -d^m(k-1) < 0$ , then the tracer moves to the following cell,
 
$$x^m(k) = x^m(k-1) + 1,$$
 and its depth is initialized with a random value uniformly distributed in the range  $[0, -D_0 d^2 h / dx^2]$ ,
 
$$d^m(k) = -uD_0 d^2 h / dx^2.$$
- (2) In any other case the tracer remains in the same cell,
 
$$x^m(k) = x^m(k-1),$$
 and its depth is updated just by adding the corresponding amount of diffusive flux (which can be a positive or negative amount),
 
$$d^m(k) = d^m(k-1) + D_0 d^2 h / dx^2.$$

The bottom line is that, only tracers that are at a depth smaller than  $N_f$  from the surface will be moved to the next cell by a passing avalanche.

The depth of the tracer at its new location will be randomly chosen in the interval between zero and  $N_f$ . The same principle holds for the diffusive contribution, but with the relevant depth being now  $-D_0 d^2 h/dx^2$ .

#### 4. Characterization of tracer transport in the diffusive sandpile

In this section, we analyze the transport of these tracers as a function of the strength of the diffusive channel relative to the avalanching one. It is worth reminding here that the sandpile domain is naturally split into an outer part where avalanche and diffusive transport coexist ( $x > x_t$ ), and an inner part ( $x < x_t$ ) where only the diffusive channel is active. As mentioned previously,  $x_t \simeq D_0(Z_c - N_f)/P_0$ .

##### 4.1. Global confinement time

The sand confinement time is defined as the ratio of the total amount of sand confined in the sandpile in a steady state to the total external power:

$$\tau^{\text{global}} = \frac{\int_0^L h(x) dx}{P_0 L}, \quad (2)$$

Physically, the global sand confinement time estimates the average time that a grain of sand spends in the pile before exiting through its bottom edge. This is a very important quantity in many applications. One such case are magnetically confined plasmas, where the global energy confinement time is the most important figure-of-merit to characterize the performance of a confining device [15]. In fact, understanding how the energy confinement time derives from the underlying transport dynamics has been one of the most active areas of research in this field for decades. Naturally, the sand confinement time is a function of the parameters that define the sandpile:  $L$ ,  $Z_c$ ,  $N_f$ ,  $P_0$  and  $D_0$ . It is straightforward to estimate it analytically [19, 15]. Indeed, the steady state profiles are, for  $x_t \leq L$ ,

$$h(x) = -\frac{P_0 x^2}{2D_0} + Z_a L - \frac{Z_a^2 D_0}{2P_0}, \quad 1 \leq x \leq x_t < L, \quad (3a)$$

$$h(x) = Z_a (L - x), \quad x_t \leq x \leq L, \quad (3b)$$

and for  $x_t \geq L$ ,

$$h(x) = -\frac{P_0}{2D_0} (x^2 - L^2), \quad 1 \leq x \leq L. \quad (4)$$

Using Eq. (2) and assuming that  $L \gg 1$ ,  $P_0 \ll 1$  and  $N_f \ll Z_a$ , one easily finds,

$$\tau_I^{\text{global}} \approx \frac{Z_a L}{2P_0} - \frac{D_0^2 Z_a^3}{6P_0^3 L}, \quad x_t \leq L, \quad (5a)$$

$$\tau_{II}^{\text{global}} \approx \frac{L^2}{3D_0}, \quad x_t \geq L. \quad (5b)$$

These formulas agree very well with the numerical values obtained with the diffusive sandpile (see Fig. 2).

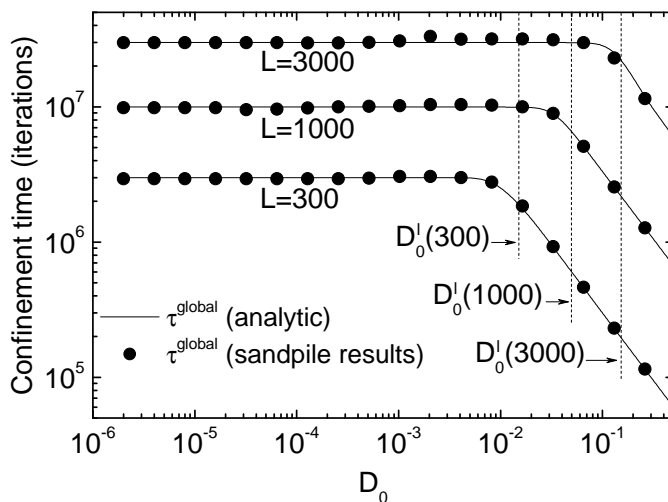


Figure 2: Tracer confinement times as a function of  $D_0$  for different sandpile lengths. Full lines and filled circles show the analytic values and the numerical estimations for  $\tau^{\text{global}}$ . Vertical lines show the limiting values for the diffusion coefficient,  $D_0^l$ , for which  $x_t \geq L$ . The parameters used for all sandpile simulations are:  $Z_c = 26$ ,  $N_f = 12$  and  $P_0 = 10^{-3}$ .

#### 4.2. Tracer particle confinement time

From the point of view of a grain, however, the confinement time is defined as the average time needed by the grain to traverse the sandpile:

$$\tau^{\text{tracer}} = \langle T_{\text{tr}} \rangle. \quad (6)$$

We will refer to it also as the transit time.

Since the width of the active layer is  $N_f$  at any cell, as mentioned previously, up to  $N_f$  different tracers can be initialized at a single cell. Thus, in order to gather meaningful statistics (that require many more tracers than

$N_f$ ), we need to initialize tracers at various cells which implies that the distances that separate them from the sandpile edge are quite different. In order to make later comparisons among different realizations more meaningful, we have introduced a normalized tracer confinement time:

$$\bar{\tau}^{\text{tracer}} = \frac{L - 1}{L - \langle x_0 \rangle} \tau^{\text{tracer}}, \quad (7)$$

where  $L$  is the number of cells of the sandpile and  $\langle x_0 \rangle$  is the average initial position. Since our tracer initializations are all random and uniformly distributed in the range  $[x_0^{\min}, x_0^{\max}]$ ,  $\langle x_0 \rangle = (x_0^{\min} + x_0^{\max})/2$ .

Figure 3 shows the normalized confinement times obtained from many simulations as a function of the diffusivity parameter,  $D_0$ . Two different types of initialization have been used in these simulations. First, in Type I initializations all tracked grains are initialized within the upper 10% of the cells. In type II runs, tracked grains are initialized within the full domain,  $[1, L]$ . The normalized confinement time obtained in each case (represented, respectively, by open and closed circles in Fig. 3) is similar, but not identical. The first thing to note in Fig. 3 is that, for diffusivities  $D_0 < 10^{-6}$  the confinement time is roughly independent of the diffusivity, but scales with the sandpile size. In particular, it can be seen that  $\bar{\tau}^{\text{tracer}} \sim L^{0.4}$ , that is consistent with the expected value for the non-diffusive sandpile [18], previously found to follow the scaling law  $\bar{\tau}^{\text{tracer}} \simeq 0.34L^{0.4}N_f/P_0$ . Transport in this regime exhibits all the classical SOC characteristics: avalanches, self-similarity, memory, and so on, that seem completely unaffected by the presence of finite diffusion.

An abrupt change in scaling is observed at around  $D_0 \sim 10^{-6}$ , for the parameters used. The confinement time is suddenly reduced, becoming independent of both diffusivity and system size. Such a dynamical transition has been known for quite some time [14], and is apparently controlled by the critical parameter  $\kappa = D_0N_f^2/P_0$ , a combination of the drive, diffusion and overturning size. The physical meaning of  $\kappa$  is related to the average roughness of the sandpile profile, quantified in terms of the variance of the height profile [20]. In our simulations, the change in behaviour takes place at  $\kappa_c \sim 22 - 24$ , consistent with the critical value ( $\kappa_c = 23$ ) reported in previous studies [14, 16]. It is also worth mentioning that the transition takes place even when the fraction of transport diffusively driven out of the sandpile,  $D_0Z_a$ , is still much lower than the integrated source,  $P_0L$ .

Transport becomes markedly different above the transition (i.e., for  $D_0 >$

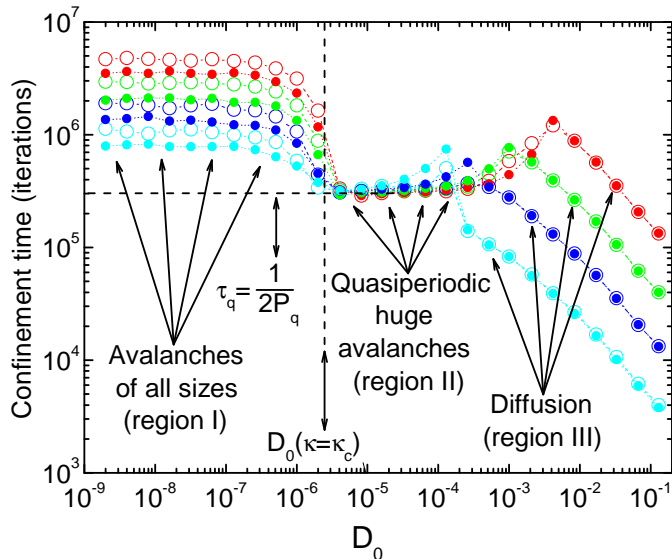


Figure 3: Normalized tracer confinement times as a function of  $D_0$  for different sandpile lengths and initializations: red ( $L = 10000$ ), green ( $L = 3000$ ), blue ( $L = 1000$ ) and cyan ( $L = 300$ ). Hollow symbols stand for initializations of the type I, whilst filled symbols stand for initializations of the type II (see in the text). The parameters in common for all simulations were:  $Z_c = 200$ ,  $N_f = 30$  and  $P_0 = 10^{-4}$ .

$D_0^{\text{II}} := D(\kappa_c) = \kappa_c P_0 / N_f^2$ ). It is now dominated by large quasi-periodic events that have an extent that covers almost completely the outer part of the sandpile,  $x > x_t$ . The frequency of these large events,  $P_q$ , can be estimated by balancing the integrated source,  $P_0 L$ , and the flux leaving the last cell [16]:

$$P_0 L \simeq D_0 Z_a + 2(L - x_t) N_f P_q. \quad (8)$$

The first and second terms in the r.h.s. of Eq. (8) represent the contributions of the two active transport channels: the diffusive one and that related to the large, quasi-periodic events. Inserting the previously obtained expressions for  $Z_a$  and  $x_t$ , it is found that:

$$P_q \simeq \frac{P_0}{2N_f} \left( \frac{1 - (D_0/P_0 L)(Z_c - N_f/2)}{1 - (D_0/P_0 L)(Z_c - N_f)} \right), \quad (9)$$

that matches very well with the frequency observed in the simulations. It should be noted that, for  $Z_c \gg N_f$ ,  $P_q \approx P_0/2N_f$ , becoming independent of the diffusivity  $D_0$ . The average confinement time in this regime seems to be

well approximated by  $\bar{\tau}^{\text{tracer}} \sim P_q^{-1}/2 \sim N_f/P_0$ , a reflection of the fact that tracers will leave the sandpile after the lapse of time that passes from the moment when they are added to the sandpile and the triggering of the next quasi-periodic event.

It is also observed in Fig. 3 that the confinement time first increases at the end of the quasi-periodic avalanche region (region II), and then decreases again. The values of  $D_0$  at which the increase and later decrease take place both increase with the system size. The explanation for this behaviour has to do with the dependencies of the transition point,  $x_t = D_0(Z_c - N_f)/P_0$ , that increases with diffusivity. Since tracked grains are always initialized at the same locations, it happens that, as the value of  $D_0$  is raised, an increasingly large number of tracers will initially fall within the inner region, where only the diffusive channel is active. As a result, these grains need a longer time to reach the outer region dominated by the quasi-periodic events. The longer, the larger the sandpile is. Since the confinement time is the sum of the time needed by the tracer to traverse the inner or diffusive region,  $\bar{\tau}_d^{\text{tracer}}$ , plus the time needed to traverse the outer region,  $\bar{\tau}_{qp}^{\text{tracer}} = N_f/P_0$ , the average time needed to exit the sandpile via quasi-periodic events becomes:

$$\bar{\tau}^{\text{tracer}} = \bar{\tau}_d^{\text{tracer}} + \bar{\tau}_{qp}^{\text{tracer}} = \bar{\tau}_d^{\text{tracer}} + \frac{N_f}{P_0}. \quad (10)$$

Finally, the last scaling region seen in Fig. 3 corresponds to the fully diffusive region (region III). That is, when  $D_0$  is sufficiently large so that  $x_t \geq L$ . Clearly, the minimum diffusivity value needed scales linearly with  $L$  since it must satisfy:

$$L \sim \frac{D_0^{\text{III}}}{P_0}(Z_c - N_f) \rightarrow D_0^{\text{III}} = \frac{P_0 L}{Z_c - N_f}. \quad (11)$$

For  $D_0 > D_0^{\text{III}}$ , only the diffusive transport channel is active. In this region, the tracer confinement time increases linearly with  $L$ , and scales as  $D_0^{-2/3}$ . This is different from the expected  $D_0^{-1}$  for pure diffusive processes, but is only due to the specific set of rules we have chosen to advance the tracked grains: only those located in the active layer of each cell are affected by avalanches and/or diffusion, whilst the rest of regular particles remain at rest (pure diffusive scalings would have indeed been recovered if tracked particles had been chosen from within the full cell population instead!). The tracer confinement times also exhibits a peak at the transition between regions

II and III ( $D_0 = D_0^{\text{III}}$ ) that deserves an explanation. In contrast to the case  $D_0 < D_0^{\text{III}}$ , in which the distance the tracers have to travel diffusively increases proportionally with increasing  $D_0$  (this distance is equal to  $x_t - x_0$  and  $x_t$  is proportional to  $D_0$ ), in the case  $D_0 \geq D_0^{\text{III}}$ , the distance that tracers have to travel diffusively does not increase with  $D_0$ , since now  $x_t > L$  and, therefore, the distance the tracers have to travel diffusively is  $L - x_0$ , no longer dependent on  $D_0$ . In these conditions, the confinement time decreases with increasing diffusion. As a side effect, a sudden disappearance of the outer region takes place, that requires that the  $N_f/P_0$  term must be dropped from  $\bar{\tau}^{\text{tracer}}$  in Eq. (10).

#### 4.3. Probability distribution function of jump-sizes

In the standard running sandpile (without diffusion), one can easily define the jumps carried out by a tracked grain as the number of cells advanced as a consequence of an avalanche that moves it down the slope. Waiting-times for the same grain are defined as the periods of time in which the grain remains at rest. In the diffusive sandpile, however, things are not so clear, since grains could still be moved by diffusion almost continuously. In order to facilitate the comparison with the standard running sandpile, we have considered that a jump starts in the diffusive sandpile when a tracked grain first changes its position as a consequence of a relaxation event, and ends when it is no longer transported by the ensuing avalanche. The size of the jump is thus given by the total number of cells traversed during the avalanche (in the same vein, a waiting-time will be defined in the next section as the number of iterations between two successive jumps, not by the extent of rest periods). Figure 4 shows the jump-size pdfs obtained for simulations with low values of  $D_0$  (region I in Fig. 3) and type I initializations (i.e., in the first 10% of the sandpile cells). These results agree with those obtained for the classical running sandpile ( $D_0 = 0$ ), that were characterized by self-similar, critical dynamics [21] (since the tail of the pdfs decay with exponents  $p(s) \sim s^{-(1+\alpha)}$  with  $0 < \alpha < 1$ ), that are only limited by the maximum jump size imposed by the finite domain of the sandpile.

Beyond the transition (i.e., for  $D_0^{\text{II}} < D_0 < D_0^{\text{III}}$ ), transport becomes dominated by near system-size, quasi-periodic avalanches previously described. Figure 5(a) shows the pdfs of the jump-sizes obtained for simulations with values of  $D_0$  within region II of Fig. 3. Here,  $x_t$  ranges from 19 to 7140. For tracers initialized within the outer region, the shape of the pdf is exponential up to jump-sizes of the order of  $L - x_0^{\text{max}}$ . Then, it becomes flattish [see Fig.

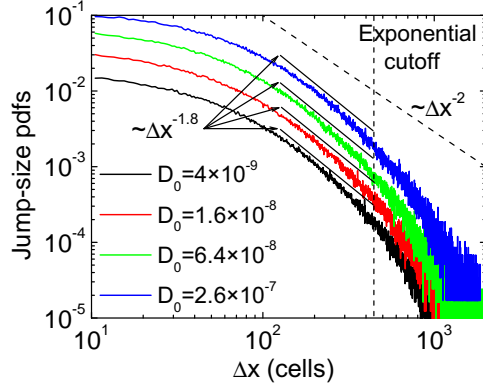


Figure 4: Pdfs for the jump-sizes of the tracked particles as they move across a diffusive sandpile. All values shown for  $D_0$  are within region I in Fig. 3. Other parameters used are:  $L = 10000$ ,  $Z_c = 200$ ,  $N_f = 30$  and  $P_0 = 10^{-4}$ . Power-law fits over the range of interest are also included.

5(b)], and ends with a peak at jump size  $L - x_t$ , vanishing for larger values. Clearly, any trace of self-similarity is now gone.

The explanation of this shape is relatively simple. First, one needs to remember that the dynamics are diffusive for  $x < x_t$ , whilst for  $x > x_t$  transport is governed by large periodic events that empty the active layer in the interval  $[x_t, L]$ . Any tracked grain initially located at  $x_0 > x_t$  will execute a single jump of length  $L - x_0$  as it is carried out of the system by a quasi-periodic event. As a result, the distribution of jump sizes will be flat between  $L - x_0^{\max}$  and  $L - x_t$  (i.e., the minimum and maximum allowable values for any jump starting at any  $x_0 > x_t$ ). The peak at jump-size  $L - x_t$  is due to the tracked grains initialized instead at  $x_0 < x_t$ . These particles must first be moved diffusively to  $x_t$ . Once there, they will execute a single jump of size  $L - x_t$  as soon as they can be transported out of the system by a quasi-periodic event. Clearly, jumps larger than  $L - x_t$  are not possible since they are limited by the size of the outer region. Finally, the exponential shape observed for jump-sizes up to  $L - x_0^{\max}$  corresponds to the smaller-size avalanches that take place in between periodic events. These avalanches are triggered randomly, a consequence of the continuous smoothing of the profiles carried out by diffusion in between quasi-periodic events, as pointed out elsewhere [14].

The behaviour of the jump-size pdfs for  $\Delta x < L - x_0^{\max}$  is well modelled by exponential functions of the type  $P(\Delta x) = A \exp(-\Delta x / \Delta x_c)$ , where

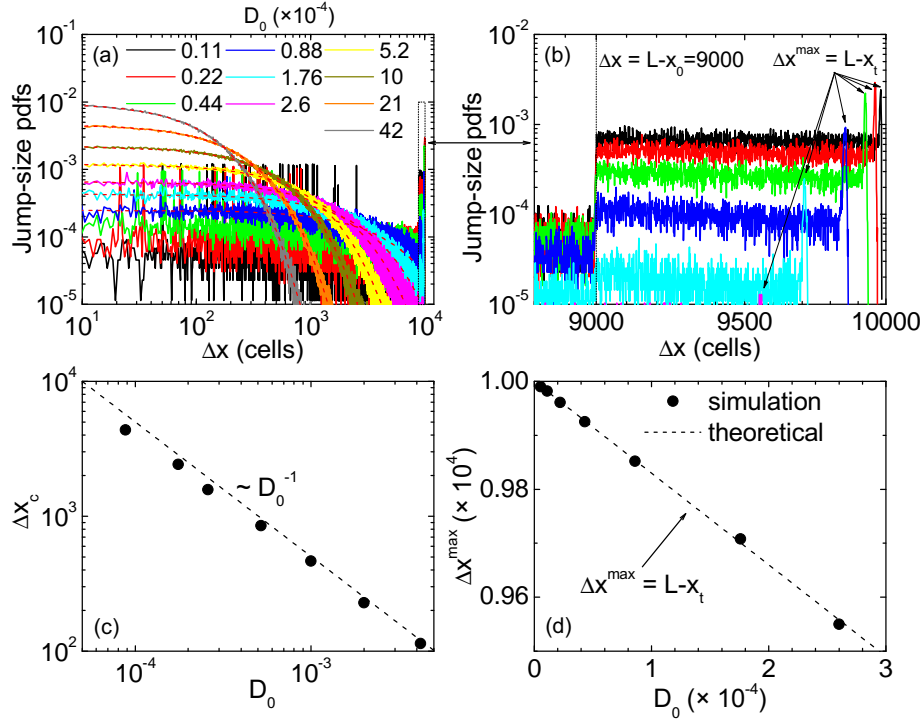


Figure 5: (a) Pdfs for the jump-sizes of the tracked particles as they move across a diffusive sandpile. All values shown for  $D_0$  are within region II in Fig. 3. The dashed region in (a) has been enlarged in (b) to better appreciate the different domains of the pdfs explained in the text. (c) Characteristic scale length for tracer jump-size pdfs when  $\Delta x < L - x_0^{\max}$  as a function of  $D_0$ . (d) Position of the peak in the jump-size pdf coming from simulations (circles). The theoretical prediction,  $\Delta x^{\max} = L - x_t$ , is also plotted (dashed line). The rest of the parameters used are the same as in Fig. 4.

$\Delta x_c$  is a scaling length for avalanches triggered in between quasi-periodic events. Exponential fits are shown in Fig. 5(a) as dashed, red lines matching quite well with the original pdfs. Figure 5(c) shows that the dependence of the exponential scaling length with diffusion is given by  $\Delta x_c \sim D_0^{-1}$ . Finally, Fig. 5(d) shows the scaling of the maximum allowable tracer jumps (i.e., the position of the peaks in jump-size pdfs) with  $D_0$ . The numerical results coming from simulations agree with the theoretical prediction given by  $\Delta x^{\max} = L - x_t = L - D_0(Z_c - N_f)/P_0$ .

For  $D_0 > D_0^{\text{III}}$ , both avalanches and quasi-periodic relaxations disappear (indeed, since  $x_t > L$ !) and transport of tracers is purely diffusive across the whole sandpile.

#### 4.4. Probability distribution function of waiting-times

We proceed now to discuss the pdfs obtained for the waiting-times between successive jumps of the tracked grains. Figure 6(a) shows the pdfs obtained for a selection of the simulations done for  $D_0 < D_0^{\text{II}}$  (i.e., inside of region I in Fig. 3) and type I initializations, using the same parameters as in the previous section. All pdfs exhibit extended power-laws with tails that

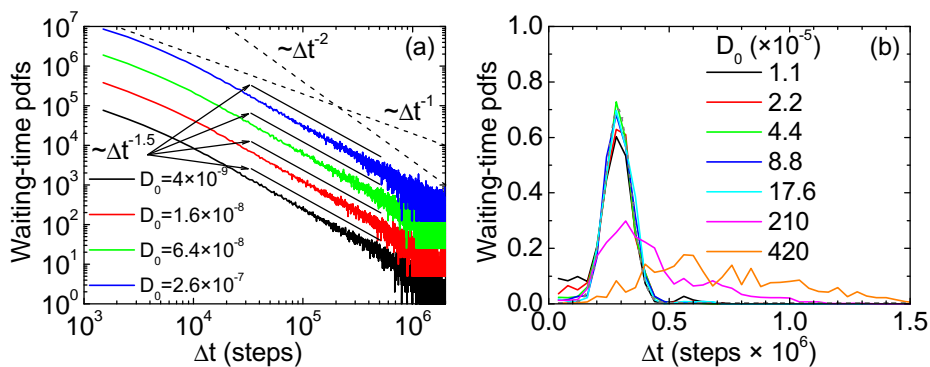


Figure 6: Pdfs for waiting-times of sand particles moving across a diffusive sandpile. In (a), all values for  $D_0$  are in the range covered by region I in Fig. 3. Power-law fits over the range of interest are also included. In (b), all values for  $D_0$  are in the range covered by region II in Fig. 3. The rest of the parameters in common in (a) and (b) were the same as in Fig. 4.

roughly decay as  $\psi(w) \sim w^{-1.5}$ , very reminiscent of the pdfs obtained for the standard running sandpile (i.e., with  $D_0 = 0$ ). This behaviour is thus indicative of the presence, for  $D < D_0^{\text{II}}$ , of the same kind of self-similar, SOC dynamics. The value of the exponent is also consistent with critical dynamics [21], that requires  $\psi(w) \sim w^{-(1+\beta)}$  with  $\beta \in (0, 1)$ . It is worth noting that, in contrast to the jump-size pdfs (see Fig. 4), where the maximum size is limited by the sandpile size  $L$ , there is no limitation here for the possible values of the waiting-times. This is the reason for not seeing any exponential cutoffs in waiting-time pdfs.

The waiting-time pdfs no longer exhibit power-law tails after the transition takes place (i.e., for  $D_0^{\text{II}} < D_0 < D_0^{\text{III}}$ ), as can be seen in Fig. 6(b). Instead, there is a well-defined peak at roughly  $w_c \sim 2.9 \times 10^5$  that, when fitted to a Gaussian law, yields a width value of about  $\sigma \simeq 5.7 \times 10^4$ . It turns out that the location of this peak is very close to the value  $P_q^{-1}/2 \sim N_f/P_0$  (equal to  $3 \times 10^5$  for the parameters used in the simulations), half of the

inverse frequency of the quasi-periodic relaxations. This was expected since tracers are being transported out of the sandpile whenever one of these events take place and, since they can be added to the system at any time, the average time they have to wait for the next relaxation to take place is half a period.

A new interesting behaviour is observed as  $D_0$  approaches the values for which the confinement time was seen to ramp up in Fig. 3. The waiting-time pdf becomes then broader and peaks at times increasingly (with  $D_0$ ) later than  $P_q^{-1}/2$  [see Fig. 6(b)]. The reason must be sought in the tracer initialization used that, for all the runs considered, takes place at values of  $x_0 \in [1, x_0^{\max}] = [1, 1000] < x_t$ , as discussed previously (for  $D_0 = 210 \times 10^{-5} \implies x_t = 3570$  and for  $D_0 = 420 \times 10^{-5} \implies x_t = 7140$ ). All tracked grains are thus initialized within the inner region, where only the diffusive transport channel is active. As a result, these grains have to travel initially only via diffusion, which increases the values of their waiting-times well beyond the maximum calculated for grains that are initialized within the interesting region, given by  $w \gg w^{\max} = P_q^{-1} \approx 6 \times 10^5$ . Additionally, the higher the diffusion, the greater the broadening of the pdf.

## 5. Effective transport models

In a recent work [18], we showed that the fractional transport equation given by,

$$\frac{\partial n}{\partial t} = {}_0D_t^{1-\beta} \left[ D_{\alpha,\beta} \frac{\partial^{\alpha,1} n}{\partial |x|^{\alpha,1}} \right] + S(x, t), \quad (12)$$

provides a good effective model for transport across the active region of the standard (i.e., non-diffusive) running sandpile in its steady state. Here,  ${}_0D_t^s$  is a Riemann-Liouville fractional derivative [17] of order  $0 < s < 1$  and start-point at  $t = 0$ , whilst  $\partial^{\alpha,1}/\partial |x|^{\alpha,1}$  is the fully asymmetrical, left-sided Riesz-Feller fractional derivative [17, 22] of order  $0 < \alpha < 1$ .  $S(x, t)$  is an external source of particles. The two fractional derivatives that appear in Eq. (12) are integro-differential operators that introduce the importance of non-locality and past-history that are characteristic of self-similar dynamics such as SOC into the transport description. The fractional exponents  $\alpha$  and  $\beta$  must be determined before the model can be used. Various ways have been proposed in the literature to do this [23, 24, 25, 13]. Probably, the optimal way is to estimate them by constructing numerically the propagator of Eq. (12). That is, the probability  $G(x, t|x', t')$  of finding a particle at location  $x$  at time  $t$  if it

was previously at  $x'$  at time  $t'$ . Tracers can be easily used for this task simply by considering the temporal evolution of an initially localised population of them. Or the temporal evolution of the distribution of population of tracers that may not be initially localized, but to whose position one subtracts their initial location. Once the propagator is available, one can estimate the values of the exponent  $\alpha$  from its asymptotic behavior at fixed time,

$$G(x, t_c | x_0, 0) \sim (x - x_0)^{-(1+\alpha)}, \quad (13)$$

for  $x - x_0 \gg D_{\alpha, \beta}^{1/\beta} t_c^{\beta/\alpha}$ , and the exponent  $\beta$  from its asymptotic behaviours at fixed position,

$$G(x_c, t | x_0, 0) \sim t^\beta, \quad \text{for } t \ll D_{\alpha, \beta}^{1/\beta} x_c^{\alpha/\beta}, \quad (14)$$

and

$$G(x_c, t | x_0, 0) \sim t^{-\beta}, \quad \text{for } t \gg D_{\alpha, \beta}^{1/\beta} x_c^{\alpha/\beta}. \quad (15)$$

In this section we use this technique to estimate  $\alpha$  and  $\beta$  for the diffusive running sandpile for values of  $D_0$  below the transition, being that the only case in which a representation such as Eq. (12) makes any sense (it is also the regime of interest for applications such as magnetically confined plasmas, where diffusion remains strongly subdominant to the avalanche channel [18]).

Figure 7(a) shows an snapshot (at fixed time,  $\Delta t = 1.6 \times 10^6$  iterations) of the propagators for six different values of  $D_0 < D_0^H$ . Each propagator is obtained by ensemble averaging 16 realizations with identical parameters. In Fig. 7(b), the same propagators have been artificially shifted by multiplying the originals successively by powers of 2 from green ( $\times 2$ ) to orange ( $\times 32$ ) in order to see more clearly the various regions where fits have been performed. The power-law fits show that all of them scale similarly. A fit such as  $G(x, t_c | x_0, 0) \sim (x - x_0)^{-1+\alpha}$  yields an average value for the spatial exponent of  $\alpha = 0.70 \pm 0.06$ .

On the other hand, Fig. 7(c) shows the growth and later decay of the propagators at a fixed location,  $\Delta x = 100$  cells, for the same diffusivities. Again, each propagator is obtained by ensemble averaging 16 realizations with identical parameters. In Fig. 7(d), the same propagators have been shifted again in the same way as in Fig. 7(b) to facilitate their analysis. Power-law fits were performed separately to the “growth” and “decay” phases, yielding a scaling  $\sim t^{0.62 \pm 0.08}$  for the growth phase, and  $\sim t^{-0.63 \pm 0.06}$  for the decay phase. Since they should theoretically correspond to the same

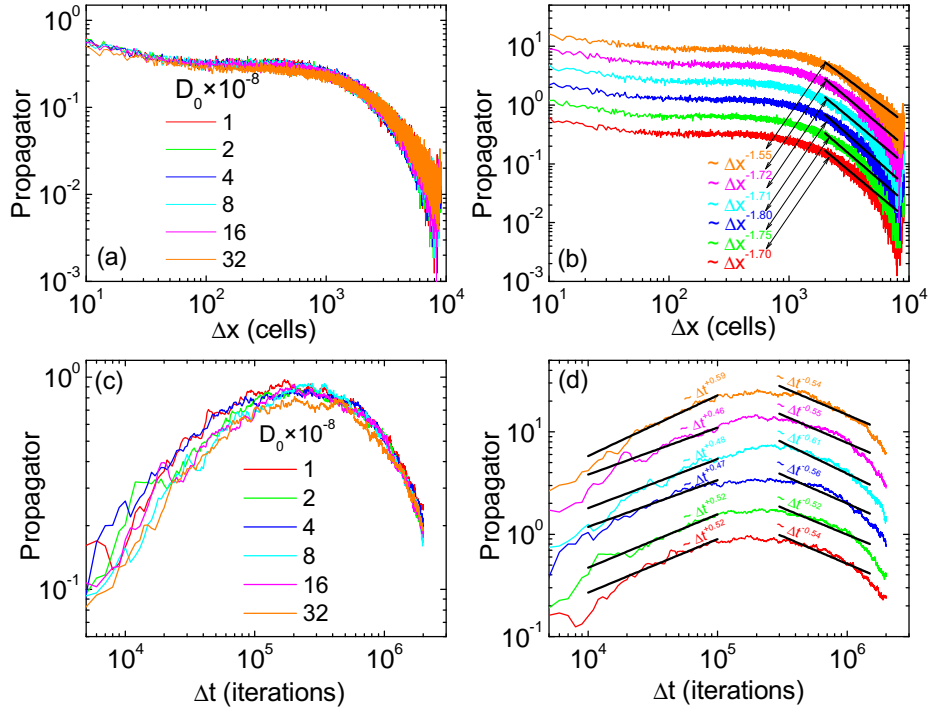


Figure 7: (a) Snapshots of the propagator at fixed time ( $1.6 \times 10^6$  iterations), for six values of  $D_0$  below the transition value ( $D_0 < D_0^{\text{II}}$ ). In (b), the same propagators have been shifted to better appreciate the power-law regions scaling as  $p(\Delta x) \sim \Delta x^{-(1+\alpha)}$ . In (c), the growth and later decay of the propagator at fixed location ( $\Delta x = 100$ ) is plotted as a function of time, for six values of  $D_0$  below the transition value. In (d), the same propagators have been shifted to better appreciate the power-law regions scaling as  $p(\Delta t) \sim \Delta t^{\pm\beta}$ . The rest of the parameters used were the same as those in the runs shown in Fig. 4.

value, their average leads to a temporal fractional exponent  $\beta \simeq 0.63 \pm 0.07$  below the transition. Figure 8 gathers all the results for both the spatial and temporal fractional exponents,  $\alpha$  and  $\beta$ , from the corresponding power-law fits of the propagators at fixed time, ( $\Delta t = 1.6 \times 10^6$  iterations), and fixed location ( $\Delta x = 100$  cells).

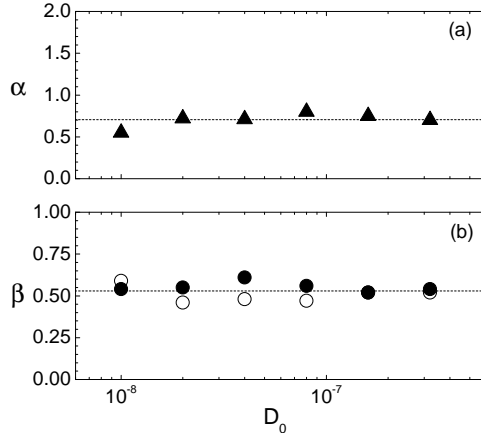


Figure 8: Summary of the results found for the spatial and temporal fractional exponents in the study of the propagator at fixed time (a) and fixed location (b), for the same diffusivities below the transition value ( $D_0 < D_0^{\text{II}}$ ) shown in Fig. 7. In (b), full circles stand for the growing phase of the propagator whilst open circles stand for the decaying phase.

It is interesting to note that the values of the fractional exponents provided by the propagator analysis,  $\alpha \sim 0.7$  and  $\beta \sim 0.6$  are not far from those that respectively describe the decay of the jump-size and waiting-time pdfs of the tracers, discussed in previous sections. This was expected since Eq. (12) can be derived [18] as the asymptotic limit of a fully asymmetric continuous-time random walk [26] defined by a jump-size distribution decaying as  $p(s) \sim s^{-(1+\alpha)}$ , with  $0 < \alpha < 1$ , and waiting-time distribution  $\psi(w) \sim w^{-(1+\beta)}$ , with  $0 < \beta < 1$ .

In regards to the situation above the transition, a fractional transport model such as Eq. (12) is no longer appropriate. In the range where transport is dominated by quasi-periodic relaxations,  $D_0^{\text{II}} < D_0 < D_0^{\text{III}}$ , there is no self-similar dynamics of any sort. A better transport model would be to consider sudden relaxations taking place with frequency  $P_q^{-1}$  that vacate the full contents of the active layer of the sandpile. In the fully diffusive region,

$D_0 > D_0^{\text{III}}$ , the effective transport model is, naturally, the usual classical diffusion equation.

## 6. Conclusions

In this work, we have characterized, by means of a collection of marked grains of sand whose individual trajectories are recorded and analyzed, the three different dynamical transport regimes that take place in the diffusive sandpile as the relative intensity of the diffusive transport channel, with respect to the avalanche-like transport channel, is increased from zero. If all other parameters that define the sandpile are kept fixed, the access to each of the three regimes only depends on the specific value of the diffusivity  $D_0$ . If  $D_0 < D_0^{\text{II}} \simeq \kappa_c P_0 / N_f^2$  (with  $\kappa_c \simeq 23$ ), the dynamics are very reminiscent of the SOC dynamics that govern the sandpile in the absence of diffusion. Transport could then be described by transport equations based on fractional differential operators, very similar to the ones used in the absence of diffusion.

For values of the diffusivity  $D_0^{\text{II}} < D_0 < D_0^{\text{III}} \simeq P_0 L / (Z_c - N_f)$ , transport across the diffusive sandpile becomes instead dominated by quasi-periodic events, and all traces of self-similarity are lost. We have shown that this change of dynamics is perfectly captured by the analysis of the tracked grains trajectories. As a result, effective transport models in terms of fractional derivatives are no longer possible, since transport is now endowed with well defined temporal and spatial scales. Namely, the period between events,  $P_q^{-1}$ , and their extension, roughly given by the size of the avalanche region,  $L - x_t$ . Finally, for  $D_0 > D_0^{\text{III}}$  the transport dynamics of the sandpile become diffusive in the traditional sense, being perfectly described by the usual diffusive equation.

## Declaration of Competing Interest

The authors declare that they have no known competing financial interests or personal relationships that could have appeared to influence the work reported in this paper.

## Acknowledgments

This research has been sponsored in part by Ministerio de Economía y Competitividad of Spain under Projects No. ENE2015-68265-P and No.

ENE2015-66444-R. Research also supported in part by DOE-OFES Grant No. DE-FG02-04ER5741 at University of Alaska. Sandpile simulations have been run in **Uranus**, a supercomputer cluster at Universidad Carlos III de Madrid (Spain) that has been funded by the Spanish Government via the national projects UNC313-4E-2361, ENE2009-12213-C03-03, ENE2012-33219 and ENE2012-31753.

## References

- [1] Bak P, Tang C, Wiesenfeld K. Self-Organized Criticality: An explanation of  $1/f$  noise. *Phys Rev Lett* 1987;59(4):381.
- [2] Lu ET, Hamilton RJ. Avalanches and the distribution of solar flares. *Astrophys J* 1991;380:L89-92.
- [3] Shaw BE, Carlson JM, Langer JS. Patterns of seismic activity preceding large earthquakes. *J Geoph Res* 1992;97(B1):479-88.
- [4] Drossel B, Schwabl F. Self-Organized critical forest-fire model. *Phys Rev Lett* 1992;69(11):1629.
- [5] Bak P, Sneppen K. Punctuated equilibrium and criticality in a simple model of evolution. *Phys Rev Lett* 1993;71(24):4083.
- [6] Mineshige S, Takeuchi M, Nishimori H. Is a black hole accretion disk in a self-organized critical state? *Astroph J* 1994;435:L125-28.
- [7] Nagatani T. Self-organized criticality in asymmetric exclusion model with noise for freeway traffic. *Physica A* 1995;218(1-2):145-54.
- [8] Field S, Witt J, Nori F, Ling X. Superconducting vortex avalanches. *Phys Rev Lett* 1995;74(7):1206.
- [9] Newman DE, Carreras BA, Diamond PH, Hahm TS. The dynamics of marginality and self-organized criticality as a paradigm for turbulent transport. *Phys Plasmas* 1996;3(5):1858-66.
- [10] Kadanoff LP, Nagel SR, Wu L, Zhou Su-min. Scaling and universality in avalanches. *Phys Rev A* 1989;39(12):6524-37.
- [11] Hwa T, Kardar M. Avalanches, hydrodynamics, and discharge events in models of sandpiles. *Phys Rev A* 1992;45(10):7002-23.

- [12] Sanchez R, Newman DE, Carreras BA. Mixed SOC diffusive dynamics as a paradigm for transport in fusion devices. *Nucl Fusion* 2001;41(3):247-56.
- [13] Sanchez R, Newman DE. Self-organized criticality and the dynamics of near-marginal turbulent transport in magnetically confined fusion plasmas. *Plasma Phys Contr Fus* 2015;57:123002.
- [14] Newman DE, Sanchez R, Carreras BA, Ferenbaugh W. Transition in the dynamics of a diffusive running sandpile. *Phys Rev Lett* 2002;88(20):204304.
- [15] Sanchez R, Newman DE, Carreras BA, Woodard R, Ferenbaugh W, Hicks HR. Modelling of ELM-like phenomena via mixed SOC-diffusive dynamics. *Nucl Fusion* 2003;43:1031-39.
- [16] Mier JA, Sanchez R, Newman DE. Characterization of a transition in the transport dynamics of a diffusive sandpile by means of recurrence quantification analysis. *Phys Rev E* 2016;94:022128.
- [17] Podlubny I. *Fractional Differential Equations*. Academic Press, New York 1998.
- [18] Sanchez R, Newman DE, Mier JA. Modeling transport across the running-sandpile cellular automaton by means of fractional transport equations. *Phys Rev E* 2018;97:052123.
- [19] Carreras BA, Lynch VE, Newman DE, Zaslaysky GM. Anomalous diffusion in a running sandpile model. *Phys Rev E* 1999;60:4770-8.
- [20] Corral A, Paczuski M. Avalanche merging and continuous flow in a sandpile model. *Phys Rev Lett* 1999;83(3):572.
- [21] Sanchez R, Newman DE. *A primer on complex systems*. Springer-Verlag, Heidelberg 2018.
- [22] Samko SG, Kilbas AA, Marichev OI. *Fractional integrals and derivatives: Theory and Applications*. Gordon and Breach Eds, New York 1993.
- [23] Metzler R, Klafter J. The random walk's guide to anomalous diffusion: A fractional dynamics approach. *Phys Rep* 2000;339:1-77.

- [24] del-Castillo-Negrete D. Fractional diffusion models of nonlocal transport. *Phys Plasmas* 2006;13(8):082308.
- [25] Mier JA, Sanchez R, Garcia L, Newman DE, Carreras BA. Characterization of nondiffusive transport in plasma turbulence via a novel lagrangian method. *Phys Rev Lett* 2008;101:165001.
- [26] Montroll EW, Weiss GH. Random walks on lattices. *J Math Phys* 1965;6(2):167.